# Global optical potential for the elastic scattering of $^{6}$He at low energies

Y. Kucuk
*Department of Physics, Giresun University, Giresun, Turkey*

I. Boztosun
*Department of Physics, Akdeniz University, Antalya, Turkey*

T. Topel
*Institute of Science, Erciyes University, Kayseri, Turkey*

(Received 23 July 2009; published 11 November 2009)

A set of global optical potentials has been derived to describe the interactions of $^{6}$He at low energies. The elastic scattering angular distribution data measured so far for many systems, ranging from $^{12}$C to $^{209}$Bi, have been considered within the framework of the optical model to find a global potential set to describe the experimental data consistently. We report that very good agreement between theoretical and experimental results has been obtained with small $\chi^2/N$ values by using the derived potential set. The reaction cross section and volume integrals of the potentials have been deduced from the theoretical calculations for all studied systems at relevant energies.

DOI: 10.1103/PhysRevC.80.054602 PACS number(s): 24.10.Ht, 24.50.+g, 25.60.−t, 25.70.−z

## I. INTRODUCTION

Defining the structure and dynamics of the halo nuclei has been a central area for nuclear physics in the past decades. Particularly, nuclear astrophysicists have been involved with the reaction mechanism of the short-lived exotic nuclei, which bear great importance because of the capture reactions that occurred in the early universe. To get more information regarding the nature of halo nuclei and their reaction mechanisms, many experiments have been carried out using radioactive ion beams (RIB) facilities. In this respect, $^{6}$He has been one of the nuclei most studied to gain an understanding of the structure of weak binding and the large radial extent to investigate the effect of the halo structure on the reaction observables [1–18]. In these works, the elastic scattering, the fusion, and the breakup/transfer cross sections have been measured and studied theoretically for many systems at energies near the Coulomb barrier to investigate the behavior of the optical potential and the effect of breakup coupling on the reaction and the scattering mechanism. The role of the Coulomb barrier and nuclear breakup on the fusion cross section has been attempted to be discovered by studying the interaction of $^{6}$He with heavy nuclei such as $^{208}$Pb, $^{209}$Bi, and $^{238}$U [9–11,19–29]. Different interpretations of how the breakup coupling affects the fusion process have been presented. These works have been extended from the heavy nuclei to weaker ones such as $^{27}$Al, $^{64}$Zn, and $^{65}$Cu and it has been observed that transfer and breakup cross sections are more important than the fusion cross sections at energies above the Coulomb barrier for weaker systems and that the total cross section of the reactions induced by halo nuclei has a large value as compared with that of the total cross section of stable nuclei reactions such as $^{4}$He and $^{6}$Li [30–32].

In addition to discussions about the reaction mechanisms of the halo nuclei, the explanation of the measured elastic scattering angular distributions near the Coulomb barrier has been the other motivation for these studies because elastic scattering holds great promise to provide information about the nuclear optical potential of the system. To observe the scattering mechanism of $^{6}$He, the experimental data for many systems including light or heavy nuclei have been analyzed by using phenomenological and microscopic potentials [33,34]. In a recent article, Milin *et al.* [34] studied the $^{6}$He + $^{12}$C system and measured the elastic and inelastic scattering as well as $2n$ transfer reaction angular distributions at $E_{\mathrm{Lab}} =$ 18.0 MeV. They analyzed these data by using the Woods-Saxon shaped phenomenological optical potential [34] and were able to obtain consistent agreement for the elastic scattering and transfer reaction data, but they were not able to obtain the inelastic $2^{+}$ data simultaneously with the elastic and transfer channel data. The same data were analyzed by Boztosun *et al.* [35]; they were able to obtain a simultaneous description of the elastic, inelastic, and transfer reaction cross sections by deforming the long-range imaginary potential within the framework of the Coupled-Channels Born Approximation (CCBA) formalism.

Studies of the elastic scattering of $^{6}$He on medium-mass target nuclei have been presented by some authors in previous years. Benjamim *et al.* [30] measured the elastic scattering angular distribution of the $^{6}$He + $^{27}$Al system using the RIBRAS (radioactive ion beams in Brazil) facilities and investigated the behavior of the total reaction cross section. They used the São Paula Potential (SPP) to reproduce the elastic scattering data and they extracted the reaction cross section for this system at several energies. For the $^{6}$He + $^{64}$Zn system, elastic scattering angular distributions, transfer/breakup angular distributions, and fusion excitation functions were measured at near Coulomb barrier energies by Di Pietro *et al.* [31] to investigate the effects of the neutron halo structure on the reaction mechanism. An optical model analysis was performed to explain the elastic scattering data and the total reaction cross section data were extracted from this analysis. Another reaction of $^{6}$He on a medium-mass target is the $^{6}$He + $^{65}$Cu system. For this system, the measured elastic scattering cross sections were analyzed using the statistical model and the

 

reaction cross sections were obtained from the theoretical results [32].

$^{6}$He + $^{208}$Pb and $^{6}$He + $^{209}$Bi are examples of systems with heavy targets that have been studied extensively to measure elastic scattering around the Coulomb barrier energies. The $^{6}$He + $^{208}$Pb system has been recently studied by Sánchez-Benítez *et al.* [29] and they have measured elastic scattering cross sections at energies between 14 and 22 MeV. In this work, the experimental data have been analyzed by using the phenomenological Woods-Saxon potential and the presence of the long-range absorption has been reported for this system. Aguilera *et al.* [9,10] for the $^{6}$He + $^{209}$Bi system have performed the simultaneous analysis of the elastic scattering and transfer reaction cross sections at energies below the Coulomb barrier by using the optical model.

As seen from the literature, $^{6}$He interactions at energies around the Coulomb barrier are crucial to understanding the properties of exotic systems and a global potential set is required in the theoretical analysis of the reactions. So far, many potential sets have been used that are either phenomenological or of the folding type to describe the elastic scattering and other scattering observables of the $^{6}$He nucleus. These potentials are very similar to those of the $^{6}$Li potentials. Sometimes, the $^{4}$He potential has also been used by adjusting the radius for the $^{6}$He one. Although a good description of the observables has been obtained by using these potentials for individual reactions, there is no global potential that describes the elastic scattering of $^{6}$He from different target nuclei consistently.

Therefore, in this article, we aim to develop a global potential set to describe the elastic scattering of the $^{6}$He nucleus from light to heavy target nuclei at low energies. In the next section, we present the optical model and introduce our global potential. The results of the theoretical analysis by using our global potential set for many systems are presented in Sec. III. We conclude in Sec. IV.

## II. OPTICAL MODEL CALCULATIONS

We have performed an extensive study of the elastic scattering of $^{6}$He on different target nuclei, from $^{12}$C to $^{209}$Bi, for a wide energy range. We have used the optical model for the theoretical calculations and the total effective potential in the optical model consists of the Coulomb, centrifugal, and nuclear potentials:

$$V_{\text{total}}(r) = V_{\text{Nuclear}}(r) + V_{\text{Coulomb}}(r) + V_{\text{Centrifugal}}(r). \quad (1)$$

In the total effective potential, the Coulomb and centrifugal potentials are well known. The Coulomb potential [36] due to a charge $Z_P e$ interacting with a charge $Z_T e$ distributed uniformly over a sphere of radius $R_c$ is given by

$$V_{\text{Coulomb}}(r) = \frac{1}{4\pi\epsilon_0}\frac{Z_P Z_T e^2}{r}, \quad r \geqslant R_c \quad (2)$$

$$= \frac{1}{4\pi\epsilon_0}\frac{Z_P Z_T e^2}{2R_c}\left(3 - \frac{r^2}{R_c^2}\right), \quad r < R_c \quad (3)$$

where $R_c$ is the Coulomb radius, taken as 1.2 fm in the calculations, and $Z_P$ and $Z_T$ denote the charges of the projectile $P$ and the target nuclei $T$, respectively.

The centrifugal potential is

$$V_{\text{Centrifugal}}(r) = \frac{\hbar^2 l(l+1)}{2\mu r^2}, \quad (4)$$

where $\mu$ is the reduced mass of the colliding pair.

Finally, the complex $V_{\text{Nuclear}}(r)$ potential is taken to be the sum of the Woods-Saxon square-shaped real and Woods-Saxon shaped imaginary potentials given as

$$V_{\text{Nuclear}}(r) = \frac{-V_0}{(1+e^{\frac{r-R_V}{a_V}})^2} + i\frac{-W_0}{1+e^{\frac{r-R_W}{a_W}}}. \quad (5)$$

Here, $R_i = r_i(A_P^{1/3} + A_T^{1/3})$ ($i = V$ or $W$), where $A_P$ and $A_T$ are the masses of projectile and target nuclei and $r_V$ and $r_W$ are the radius parameters of the real and imaginary parts of the nuclear potential, respectively.

By taking free parameters of the depth of the real and imaginary potentials, we investigated their radii for each part, which gives the best fit for the elastic scattering cross section data. To do this, we made a $\chi^2$ search. The radii of real ($r_V$) and imaginary potentials ($r_W$) were varied on a grid, from 0.5 to 2.0 fm, with steps of 0.1 fm to obtain the best fit to the data [37]. The results of this systematic search are shown in Fig. 1, which is a three-dimensional plot of $r_V$, $r_W$, and $1/\chi^2$, where $\chi^2$ has the usual definition and measures the quality of the fit. In Fig. 1, the best-fit parameters, producing oscillating cross sections with reasonable phase and period, correspond to low $\chi^2$ values and peaks in the $1/\chi^2$ surface. For the four different reactions, the figures present discrete peaks (or hills) for correlated $r_V$ and $r_W$ values, which are best-fit real and imaginary potential families and indicate that the $r_V$ or $r_W$ parameters cannot be varied continuously and still find equally satisfying fits. For the radius of the real part ($r_V$), the lowest $\chi^2$ values are generally obtained around 0.9 fm and for the radius of the imaginary part ($r_W$) they are around 1.50 fm. The diffusion parameters were also fixed, $a_V = a_W = 0.7$ fm, for both parts of the potential.

Having obtained the best fit for all data, we investigated the change of the depth of the real and imaginary parts and we derived Eqs. (6) and (7) for the variation of the depth of the real and imaginary parts of the nuclear potential. Equations depend on the incident energy of the projectile ($^{6}$He) with the charge number ($Z$) and the mass number ($A$) of the target.

$$V_0 = 110.1 + 2.1\frac{Z_T}{A_T^{1/3}} + 0.65\,E, \quad (6)$$

$$W_0 = 6.0 + 0.48\frac{Z_T}{A_T^{1/3}} - 0.15\,E, \quad (7)$$

where $E$ is the laboratory energy of $^{6}$He and $Z_T$ and $A_T$ are the charge and mass numbers of the target nuclei.

For the $^{6}$He + $^{208}$Pb system, the real and imaginary potentials are shown in Fig. 2 for $E_{\text{Lab}} = 18.0$ MeV. The sum of the nuclear, the Coulomb, and the centrifugal potentials is also shown in the same figure for the orbital angular momentum quantum numbers, $l = 0$ to 50. The superposition of the attractive and repulsive potentials results in the formation of a potential pocket, in which the width and the depth of the pocket

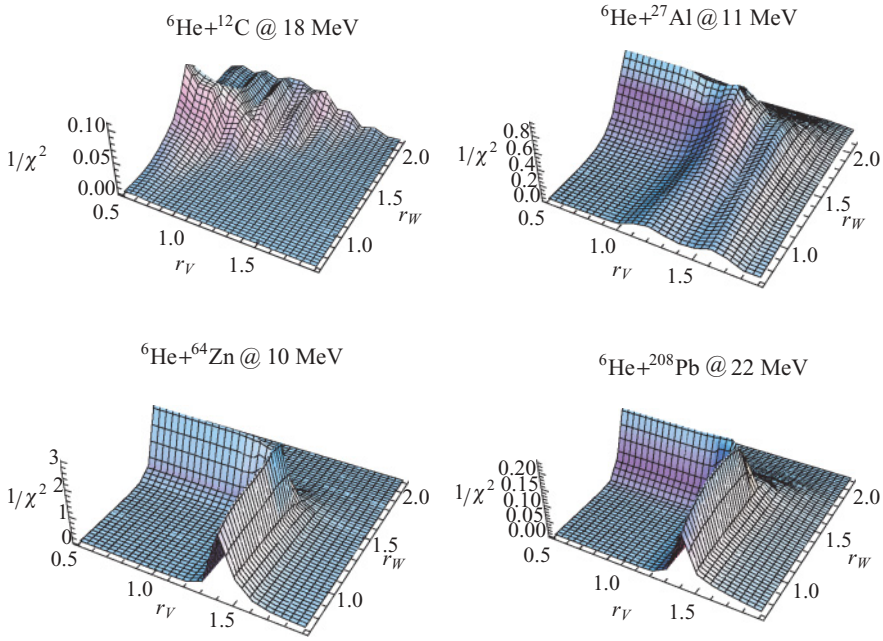


FIG. 1. (Color online) Three-dimensional plots of the optical model parameters $r_V$, $r_W$, and $1/\chi^2$, where $\chi^2$ has the usual definition and measures the quality of the fit.

depend on the orbital angular momentum. It is well known that this pocket is very important for the interference of the barrier and internal waves, which produces the pronounced structure in the cross section [38,39]. We perceive from Fig. 2 that the real part is located inside the imaginary one, which shows that the long-range absorption is needed to explain the interaction of $^6$He.

## III. RESULTS

We analyzed the elastic scattering of $^6$He from target nuclei $^{12}$C, $^{27}$Al, $^{58}$Ni, $^{64}$Zn, $^{65}$Cu, $^{197}$Au, $^{208}$Pb, and $^{209}$Bi for a wide energy range below 50 MeV by using the derived new optical potential set given by Eqs. (6) and (7) within the framework of the optical model.

The first system we considered was $^6\mathrm{He} + {}^{12}\mathrm{C}$ elastic scattering, an example of a light-heavy target; we analyzed this system at energies of 8.79, 9.18, and 18.0 MeV in the laboratory system. The experimental data for 8.79 and 9.18 MeV were measured by Smith *et al.* [33] and were analyzed by using the potential parameters of $^4$He, $^6$Li, and $^7$Li. In their work, the angular distribution of $^6$He was well produced by using $^6$Li and $^7$Li optical potential parameters, whereas the $^4$He parameters did not produce the data well. In our study, the elastic scattering data at these energies as well as the data at 18.0 MeV measured by Milin *et al.* [34] were analyzed by using the new potential and a good agreement was obtained for all energies as presented in Fig. 3. When the theoretical results are compared with experimental data, we have obtain small $\chi^2/N$ values as seen in Table I. In the same table, we also present the prediction of the new potential parameters for the reaction cross sections. The values are comparable with those of more sophisticated Continuum Discretized Coupled Channels (CDCC) or similar approaches.

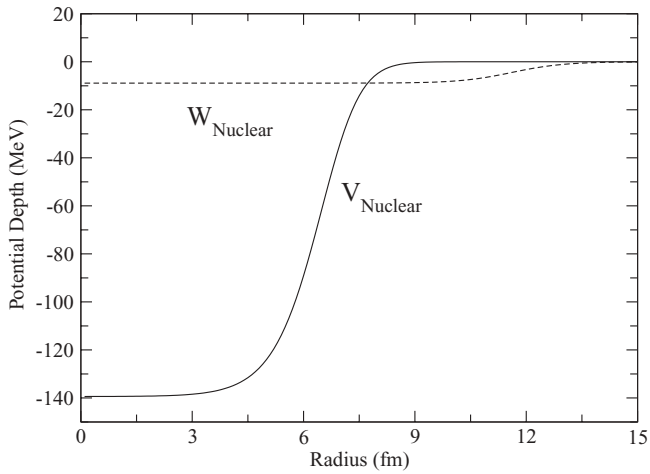


FIG. 2. The real (solid line) and imaginary (dashed line) parts of the nuclear potential at $E_{\mathrm{Lab}} = 18$ MeV for $^6\mathrm{He} + {}^{208}\mathrm{Pb}$.

Another studied system is the $^6\mathrm{He} + {}^{27}\mathrm{Al}$ reaction. Elastic scattering data of this system have been measured by Benjamim *et al.* [30] at energies of 9.5, 11.0, 12.0, and 13.4 MeV using the RIBRAS facilities. They have also analyzed the measured data theoretically by using the SPP and they have also deduced the reaction cross sections from the optical model fits. They have predicted the reaction cross sections for these energies as 1110, 1257, 1300, and 1327 mb, respectively. In comparing our results with these values, we see a difference of about 200 mb between the microscopic potentials and our phenomenological potentials. The difference is due to the shape of the imaginary potential. The theoretical results of our potential for $^6\mathrm{He} + {}^{27}\mathrm{Al}$ elastic scattering and the extracted reaction cross sections for each energy are given in Table I and Fig. 4.

For the medium-mass target, $^{58}$Ni, $^{64}$Zn, and $^{65}$Cu have been analyzed by using the optical potential parameters obtained from the potential formula [Eqs. (6) and (7)]. These systems have been studied around the Coulomb barrier and the elastic scattering cross sections have been measured by Refs. [17,31,32]. For the $^6\mathrm{He} + {}^{64}\mathrm{Zn}$ system, the reaction cross

TABLE I. The reaction cross section, volume integrals, and $\chi^2/N$ values obtained by using the experimental error bars.

| | $E$ (MeV) | $\chi^2/N$ | $\sigma_R$ (mb) | $J_V$ (MeV fm$^3$) | $J_W$ (MeV fm$^3$) | | $E$ (MeV) | $\chi^2/N$ | $\sigma_R$ (mb) | $J_V$ (MeV fm$^3$) | $J_W$ (MeV fm$^3$) |
|---|---|---|---|---|---|---|---|---|---|---|---|
| $^{12}$C | 8.79 | 4.76 | 1241 | 256.24 | 90.91 | $^{27}$Al | 9.5 | 1.14 | 1237 | 193.22 | 70.87 |
| | 9.18 | 2.52 | 1262 | 256.79 | 90.14 | | 11.0 | 1.61 | 1380 | 194.71 | 68.42 |
| | 18.0 | 26.30 | 1453 | 268.90 | 69.75 | | 12.0 | 4.25 | 1453 | 195.71 | 66.82 |
| | | | | | | | 13.4 | 2.29 | 1531 | 197.12 | 64.58 |
| $^{64}$Zn | 10.0 | 0.40 | 537.5 | 155.73 | 62.35 | $^{65}$Cu | 22.6 | 36.27 | 2012 | 163.95 | 46.53 |
| $^{58}$Ni | 9.0 | 1.63 | 383.1 | 158.63 | 64.73 | $^{197}$Au | 27.0 | 13.12 | 1925 | 141.2 | 46.70 |
| | | | | | | | 40.0 | 0.51 | 2843 | 148.88 | 35.94 |
| $^{208}$Pb | 14.0 | 0.75 | 3.935 | 132.69 | 57.39 | $^{209}$Bi | 14.7 | 19.87 | 9.190 | 133.25 | 67.10 |
| | 16.0 | 3.11 | 59.71 | 133.85 | 55.76 | | 16.3 | 14.93 | 64.01 | 134.15 | 55.85 |
| | 18.0 | 3.23 | 302.3 | 135.02 | 54.12 | | 17.8 | 11.40 | 235.7 | 135.05 | 54.60 |
| | 22.0 | 5.05 | 1118 | 137.34 | 50.85 | | 19.0 | 2.27 | 454.6 | 135.70 | 53.62 |
| | 27.0 | 5.70 | 1892 | 140.71 | 46.82 | | 22.5 | 2.25 | 1168 | 137.78 | 50.74 |

sections have been deduced as $380 \mp 60$ mb for 10.0 MeV and $1450 \mp 130$ mb for 13.6 MeV using the phenomenological potential set by Ref. [31]. These values are comparable with our results with a difference of around 10%. The results of our potential for the elastic scattering of these reactions and the reaction cross section values for each energy are given in Table I and Fig. 5.

We have also studied the elastic scattering of $^6$He from heavy targets such as $^{197}$Au, $^{208}$Pb, and $^{209}$Bi. For these systems, the elastic scattering angular distributions have been measured at energies near the Coulomb barrier generally. Kakuee *et al.* [12] have measured the elastic scattering cross section of $^6$He + $^{197}$Au and $^6$He + $^{208}$Pb at 27.0 MeV and they have analyzed the data by using the optical model. In their calculations, they have used the parameters that fit the $^6$Li systems by both taking into account and ignoring the dipole polarizability. However, because this potential set was not adequate to fit the data, they have modified the potential by changing the depth and diffuseness of the real potential. They have shown that large imaginary diffuseness

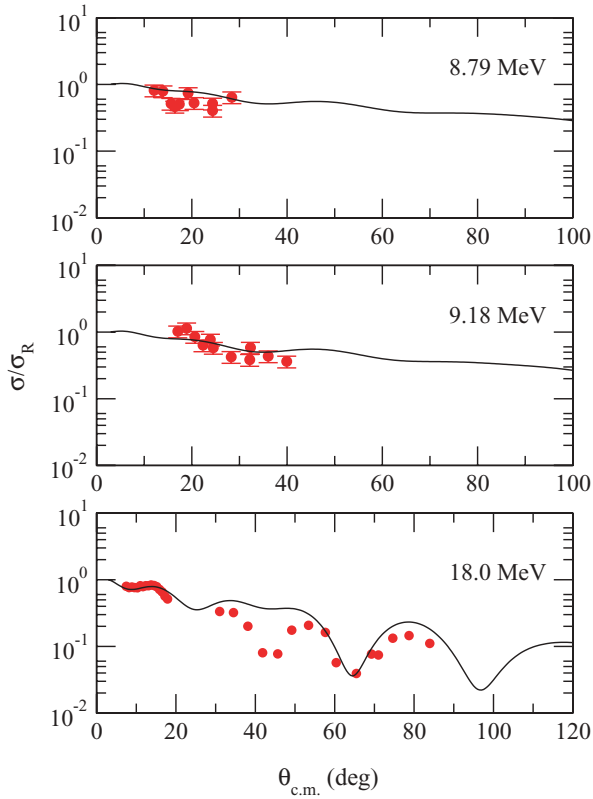


FIG. 3. (Color online) Elastic scattering angular distributions for $^6$He + $^{12}$C. The solid lines show OM calculation results while the circles show the experimental data. The experimental data have been taken from Refs. [33] and [34].

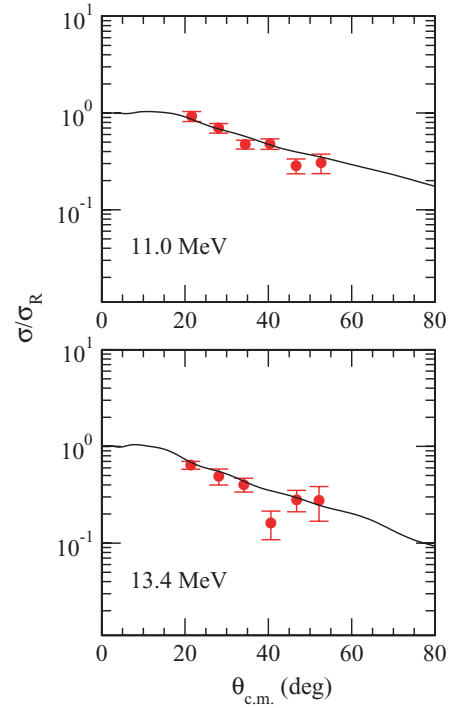


FIG. 4. (Color online) Elastic scattering angular distributions (ratio to Rutherford cross section) for $^6$He + $^{27}$Al. The solid lines show OM calculation results while the circles show the experimental data. The experimental data have been taken from Ref. [30].

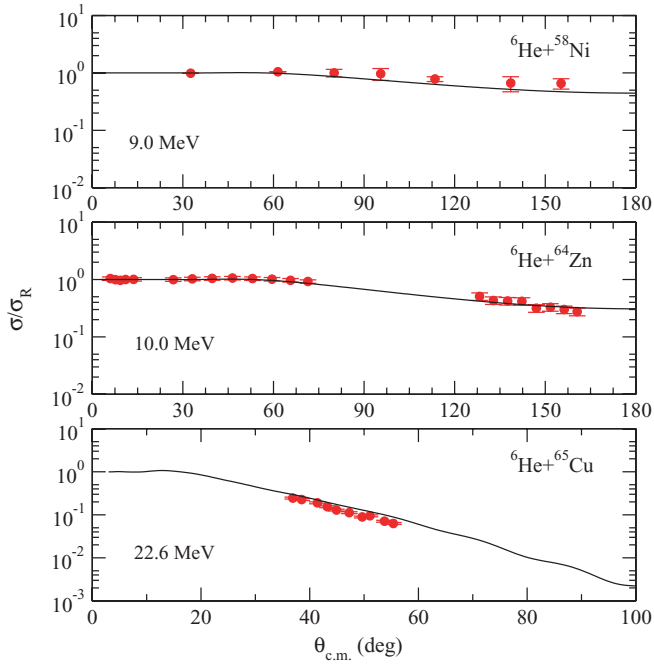


FIG. 5. (Color online) Elastic scattering angular distributions (ratio to Rutherford cross section) for $^{6}$He + $^{58}$Ni, $^{64}$Zn, and $^{65}$Cu. The solid lines show OM calculation results while the circles show the experimental data. The experimental data have been taken from Refs. [17,18,31,32].

parameters are required to fit the experimental data and they have presented these results as evidence of the long-range absorbtion mechanism. In this work, they have found the reaction cross section around 1900 mb at 27 MeV, which is estimated due to Coulomb breakup. In comparing this work with our calculations, we observe the same results. Our potential produces the reaction cross sections as 1925 and 1892 mb for $^{197}$Au and $^{208}$Pb nuclei at 27 MeV, respectively.

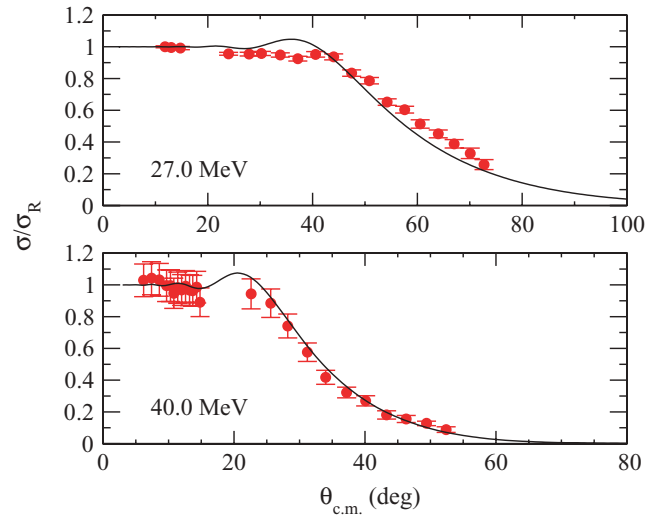


FIG. 6. (Color online) Elastic scattering angular distribution (ratio to Rutherford cross section) for $^{6}$He + $^{197}$Au. The solid lines show OM calculation results while the circles show the experimental data. The experimental data have been taken from Refs. [12] and [14].

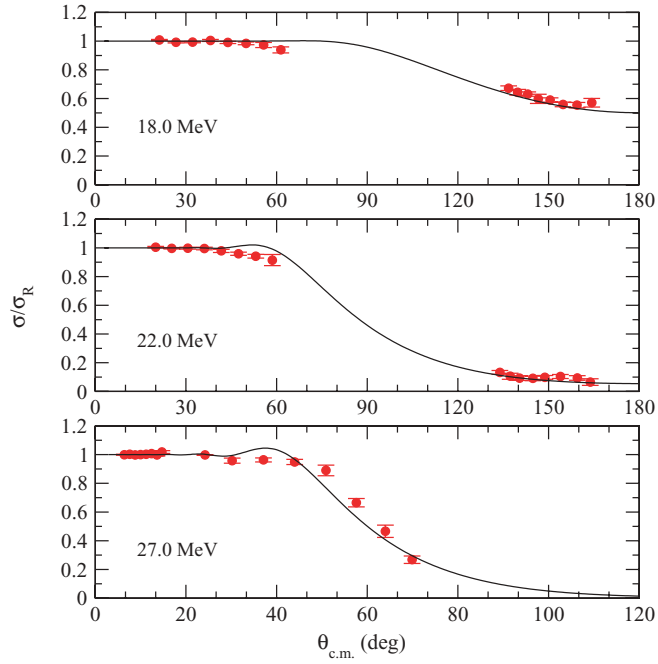


FIG. 7. (Color online) Elastic scattering angular distribution (ratio to Rutherford cross section) for $^{6}$He + $^{208}$Pb. The solid lines show OM calculation results while the circles show the experimental data. The experimental data have been taken from Refs. [8] and [13].

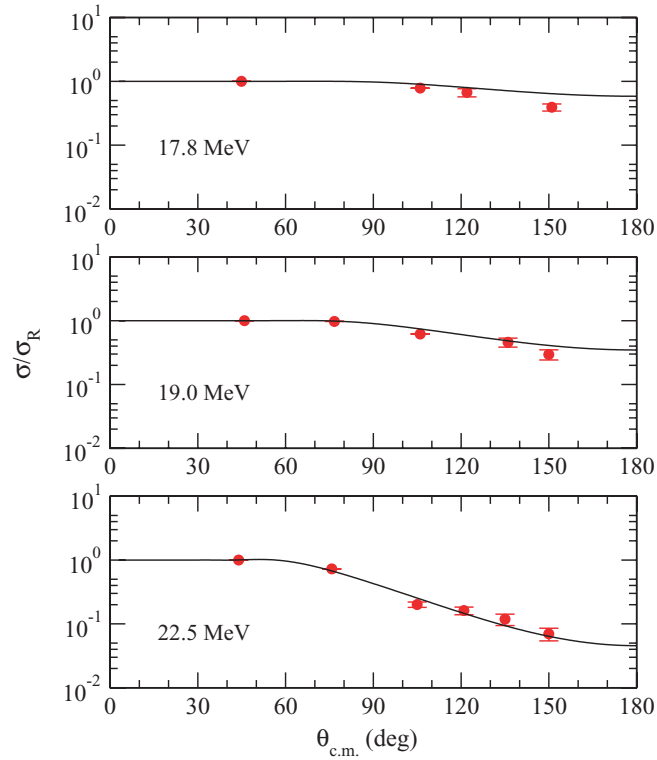


FIG. 8. (Color online) Elastic scattering angular distribution (ratio to Rutherford cross section) for $^{6}$He + $^{209}$Bi. The solid lines show OM calculation results while the circles show the experimental data. The experimental data have been taken from Refs. [9] and [10].

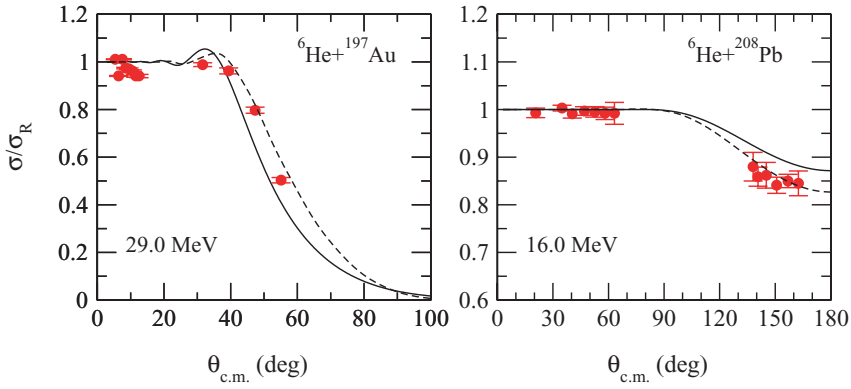


FIG. 9. (Color online) Elastic scattering angular distribution (ratio to Rutherford cross section) for $^6$He + $^{197}$Au and $^6$He + $^{208}$Pb. The solid lines show OM calculation results with the imaginary potential of Eq. (7) while the dashed lines show a decrease (left panel) and an increase (right panel) of 5 MeV from the value of Eq. (7).

It also gives good results for elastic scattering with very small $\chi^2/N$ values as shown in Figs. 6 and 7 and Table I. In addition, the elastic scattering cross sections of $^6$He + $^{208}$Pb and $^6$He + $^{209}$Bi for 11 different energies conducted in the literature [9,10,29] have been studied and excellent agreement has been obtained for experimental data. The results for some of these energies are given in Figs. 7 and 8.

We should point out that although the new potential set provides a consistent agreement for many systems, the potential parameters need a small modification to fit the experimental data at some energies for heavy targets. As seen in Fig. 9, while the new potential predicts the behavior of the cross section, it cannot fit the data exactly: It over/underestimates the experimental data in particular cases. However, a change of the depth of the imaginary potential such as ±5 MeV is sufficient to fit the data.

In Table I, for all the reactions we have studied in this article, we have presented the $\chi^2/N$ values, the reaction cross section values, and the volume integrals produced by the new potential set. For the theoretical calculations, the code FRESCO [40] has been used.

## IV. CONCLUSION

We have presented a new potential set by deriving a formula for the depth of the real and imaginary parts of the optical potential for $^6$He elastic scattering at low energies. We should point out that we do not aim to obtain the best fits for the experimental data. Rather, we attempt to derive a global potential set that produces the behavior of the experimental data reasonably well. In this sense, we have analyzed almost all the experimental data conducted over a wide energy range in the literature by using this potential set to show the validity of the potential in explaining the elastic scattering data and reasonable agreement has been obtained for all data with reasonable $\chi^2/N$ values.

As can be seen from our results obtained by using the new potential parameters, one can easily use this potential set instead of using the improved parameters of the most similar nuclei such as $^4$He, $^6$Li, and $^7$Li as is most commonly done. This global potential can also be extended to describe the scattering observables of other halo-type nuclei, which is important in providing information regarding their interaction mechanism.

## ACKNOWLEDGMENTS

This work has been supported by the Turkish Science and Research Council (TÜBİTAK) under Grant 107T824, the Turkish Academy of Sciences (TÜBA-GEBİP), and the Akdeniz University Scientific Research Projects Unit.

[1] J. S. Al-Khalili, M. D. Cortina-Gil, P. Roussel-Chomaz, N. Alamanos, J. Barrette, W. Mittig, F. Auger, Y. Blumenfeld, J. M. Casandjian, M. Chartier, V. Fekou-Youmbi, B. Fernandez, N. Frascaria, A. Gillibert, H. Laurent, A. Lepine-Szily, N. A. Orr, V. Pascalon, J. A. Scarpaci, and J. L. Sida, Phys. Lett. **B378**, 45 (1996).
[2] J. S. Al-Khalili, J. A. Tostevin, and I. J. Thompson, Phys. Rev. C **54**, 1843 (1996).
[3] S. Karataglidis, P. J. Dortmans, K. Amos, and C. Bennhold, Phys. Rev. C **61**, 024319 (2000).
[4] Y. Suzuki, Nucl. Phys. **A528**, 395 (1991).
[5] K. Varga, Y. Suzuki, and Y. Ohbayasi, Phys. Rev. C **50**, 189 (1994).
[6] S. Funada, H. Kameyama, and Y. Sakuragi, Nucl. Phys. **A575**, 93 (1994).
[7] P. Navratil, W. E. Ormand, E. Caurier, and C. Bertulani, Lawrence Livermore National Laboratory, UCRL-PROC-211912 (2005). DOE Contract Number W-7405-ENG-48.
[8] A. M. Sánchez-Benítez, D. Escrig, M. A. G. Alvarez, M. V. Andres, C. Angulo, M. J. G. Borge, J. Cabrera, S. Cherubini, J. M. Espino, P. Figuera, M. Freer, J. E. Garcia-Ramos, J. Gomez-Camacho, M. Gulino, O. R. Kakuee, I. Martel, C. Metelco, A. M. Moro, J. Rahighi, K. Rusek, D. Smirnov, O. Tengblad, P. Van Duppen, and V. Ziman, J. Phys. G: Nucl. Part. Phys. **31**, S1953 (2005).
[9] E. F. Aguilera, J. J. Kolata, F. M. Nunes, F. D. Becchetti, P. A. DeYoung, M. Goupell, V. Guimaraes, B. Hughey, M. Y. Lee, D. Lizcano, E. Martinez-Quiroz, A. Nowlin, T. W. O'Donnell, G. F. Peaslee, D. Peterson, P. Santi, and R. White-Stevens, Phys. Rev. Lett. **84**, 5058 (2000).

[10] E. F. Aguilera, J. J. Kolata, F. D. Becchetti, P. A. De Young, J. D. Hinnefeld, A. Horvath, L. O. Lamm, Hye-Young Lee, D. Lizcano, E. Martinez-Quiroz, P. Mohr, T. W. O'Donnell, D. A. Roberts, and G. Rogachev, Phys. Rev. C **63**, 061603(R) (2001).

[11] J. J. Kolata, V. Guimaraes, D. Peterson, P. Santi, R. White-Stevens, P. A. DeYoung, G. F. Peaslee, B. Hughey, B. Atalla, M. Kern, P. L. Jolivette, J. A. Zimmerman, M. Y. Lee, F. D. Becchetti, E. F. Aguilera, E. Martinez-Quiroz, and J. D. Hinnefeld, Phys. Rev. Lett. **81**, 4580 (1998).

[12] O. R. Kakuee, M. A. G. Alvarez, M. V. Andres, S. Cherubini, T. Davinson, A. Di Pietro, W. Galster, J. Gomez-Camacho, A. M. Laird, M. Lamehi-Rachti, I. Martel, A. M. Moro, J. Rahighi, A. M. Sánchez-Benítez, A. C. Shotter, W. B. Smith, J. Vervier, and P. J. Woods, Nucl. Phys. **A765**, 294 (2006).

[13] O. R. Kakuee, J. Rahighi, A. M. Sánchez-Benítez, M. V. Andres, S. Cherubini, T. Davinson, W. Galster, J. Gomez-Camacho, A. M. Laird, M. Lamehi-Rachti, I. Martel, A. C. Shotter, W. B. Smith, J. Vervier, and P. J. Woods, Nucl. Phys. **A728**, 339 (2003).

[14] R. Raabe, Ph.D. thesis, Katholieke Universiteit Leuven, 2001.

[15] L. Borowska, K. Terenetsky, V. Verbitsky, and S. Fritzsche, Phys. Rev. C **76**, 034606 (2007).

[16] A. A. Korsheninnikov, E. A. Kuzmin, E. Yu. Nikolskii, C. A. Bertulani, O. V. Bochkarev, S. Fukuda, T. Kobayashi, S. Momota, B. G. Novatskii, A. A. Ogloblin, A. Ozawa, V. Pribora, I. Tanihata, and K. Yoshida, Nucl. Phys. **A616**, 189 (1997).

[17] L. R. Gasques, L. C. Chamon, D. Pereira, V. Guimaraes, A. Lepine-Szily, M. A. G. Alvarez, E. S. Rossi Jr., C. P. Silva, B. V. Carlson, J. J. Kolata, L. Lamm, D. Peterson, P. Santi, S. Vincent, P. A. De Young, and G. Peasley, Phys. Rev. C **67**, 024602 (2003).

[18] R. E. Warner, F. D. Becchetti, J. W. Janecke, D. A. Roberts, D. Butts, C. L. Carpenter, J. M. Fetter, A. Muthukrishnan, J. J. Kolata, K. Lamkin, M. Belbot, M. Zahar, A. Galonsky, K. Ieki, and P. Zecher, Phys. Rev. C **51**, 178 (1995).

[19] P. A. De Young, Patrick J. Mears, J. J. Kolata, E. F. Aguilera, F. D. Becchetti, Y. Chen, M. Cloughesy, H. Griffin, C. Guess, J. D. Hinnefeld, H. Jiang, Scott R. Jones, U. Khadka, D. Lizcano, E. Martinez-Quiroz, M. Ojaniega, G. F. Peaslee, A. Pena, J. Rieth, S. Van Den Driessche, and J. A. Zimmerman, Phys. Rev. C **71**, 051601(R) (2005).

[20] M. Trotta, J. L. Sida, N. Alamanos, A. Andreyev, F. Auger, D. L. Balabanski, C. Borcea, N. Coulier, A. Drouart, D. J. C. Durand, G. Georgiev, A. Gillibert, J. D. Hinnefeld, M. Huyse, C. Jouanne, V. Lapoux, A. Lepine, A. Lumbroso, F. Marie, A. Musumarra, G. Neyens, S. Ottini, R. Raabe, S. Ternier, P. Van Duppen, K. Vyvey, C. Volant, and R. Wolski, Phys. Rev. Lett. **84**, 2342 (2000).

[21] R. Raabe, J. L. Sida, J. L. Charvet, N. Alamanos, C. Angulo, J. M. Casandjian, S. Courtin, A. Drouart, D. J. C. Durand, P. Figuera, A. Gillibert, S. Heinrich, C. Jouanne, V. Lapoux, A. Lepine-Szily, A. Musumarra, L. Nalpas, D. Pierroutsakou, M. Romoli, K. Rusek, and M. Trotta, Nature (London) **431**, 823 (2004).

[22] J. J. Kolata, H. Amro, F. D. Becchetti, J. A. Brown, P. A. De Young, M. Hencheck, J. D. Hinnefeld, G. F. Peaslee, A. L. Fritsch, C. Hall, U. Khadka, P. J. Mears, P. O'Rourke, D. Padilla, J. Rieth, T. Spencer, and T. Williams, Phys. Rev. C **75**, 031302(R) (2007).

[23] N. Keeley, J. M. Cook, K. W. Kemper, B. T. Roeder, W. D. Weintraub, F. Marechal, and K. Rusek, Phys. Rev. C **68**, 054601 (2003).

[24] R. S. Mackintosh and N. Keeley, Phys. Rev. C **70**, 024604 (2004).

[25] N. Keeley and R. S. Mackintosh, Phys. Rev. C **71**, 057601 (2005).

[26] T. Matsumoto, T. Egami, K. Ogata, Y. Iseri, M. Kamimura, and M. Yahiro, Phys. Rev. C **73**, 051602(R) (2006).

[27] L. F. Canto, P. R. S. Gomes, R. Donangelo, and M. S. Hussein, Phys. Rep. **424**, 1 (2006).

[28] L. F. Canto, R. Donangelo, P. Lotti, and M. S. Hussein, Phys. Rev. C **52**, R2848 (1995).

[29] A. M. Sánchez-Benítez, D. Escrig, M. A. G. Álvarez, M. V. Andrés, C. Angulo, M. J. G. Borge, J. Cabrera, S. Cherubini, P. Demaret, J. M. Espino, P. Figuera, M. Freer, J. E. García-Ramos, J. Gómez-Camacho, M. Gulino, O. R. Kakuee, I. Martel, C. Metelko, A. M. Moro, F. Pérez-Bernal, J. Rahighi, K. Rusek, D. Smirnov, O. Tengblad, P. Van Duppen, and V. Ziman, Nucl. Phys. **A803**, 30 (2008).

[30] E. A. Benjamim, A. Lepine-Szily, D. R. Mendes Junior, R. Lichtenthaler, V. Guimaraes, P. R. S. Gomes, L. C. Chamon, M. S. Hussein, A. M. Moro, A. Arazi, I. Padron, J. Alcantara Nunez, M. Assuncao, A. Barioni, O. Camargo Jr., R. Z. Denke, P. N. de Faria, and K. C. C. Pires, Phys. Lett. **B647**, 30 (2007).

[31] A. Di Pietro, P. Figuera, F. Amorini, C. Angulo, G. Cardella, S. Cherubini, T. Davinson, D. Leanza, J. Lu, H. Mahmud, M. Milin, A. Musumarra, A. Ninane, M. Papa, M. G. Pellegriti, R. Raabe, F. Rizzo, C. Ruiz, A. C. Shotter, N. Soic, S. Tudisco, and L. Weissman, Phys. Rev. C **69**, 044613 (2004).

[32] A. Chatterjee, A. Navin, A. Shrivastava, S. Bhattacharyya, M. Rejmund, N. Keeley, V. Nanal, J. Nyberg, R. G. Pillay, K. Ramachandran, I. Stefan, D. Bazin, D. Beaumel, Y. Blumenfeld, G. de France, D. Gupta, M. Labiche, A. Lemasson, R. Lemmon, R. Raabe, J. A. Scarpaci, C. Simenel, and C. Timis, Phys. Rev. Lett. **101**, 032701 (2008).

[33] R. J. Smith, J. J. Kolata, K. Lamkin, A. Morsad, K. Ashktorab, F. D. Becchetti, J. A. Brown, J. W. Janecke, W. Z. Liu, and D. A. Roberts, Phys. Rev. C **43**, 761 (1991).

[34] M. Milin, S. Cherubini, T. Davinson, A. Di Pietro, P. Figuera, D. Miljanić, A. Musumarra, A. Ninane, A. N. Ostrowski, M. G. Pellegriti, A. C. Shotter, N. Soić, C. Spitaleri, and M. Zadro, Nucl. Phys. **A730**, 285 (2004).

[35] I. Boztosun, M. Karakoc, and Y. Kucuk, Phys. Rev. C **77**, 064608 (2008).

[36] G. R. Satchler, *Direct Nuclear Reactions* (Oxford University Press, Oxford, 1983).

[37] Y. Kucuk and I. Boztosun, Nucl. Phys. **A764**, 160 (2006).

[38] D. M. Brink and N. Takigawa, Nucl. Phys. **A279**, 159 (1977).

[39] I. Boztosun, Phys. Rev. C **66**, 024610 (2002).

[40] I. J. Thompson, Comput. Phys. Rep. **7**, 167 (1988).